Tb_2O_3 thin films: An alternative candidate for high-k dielectric applications

Nathan W. Gray, Megan C. Prestgard, and Ashutosh Tiwari[a)]
Nanostructured Materials Research Laboratory, Department of Materials Science and Engineering, University of Utah, Salt Lake City, Utah 84112, USA

(Received 23 August 2014; accepted 19 November 2014; published online 2 December 2014)

We are reporting the growth and structural, optical, and dielectric properties of Tb_2O_3, a relatively unexplored high-k dielectric material. A pulsed-laser deposition technique was used to grow Tb_2O_3 thin-films on four different substrates: Si(100), $SrTiO_3$(100), $LaAlO_3$(100), and MgO(100). High-resolution X-ray diffraction and transmission electron microscopy results confirmed that film growth in an oxygen-rich (10^{-1} Torr) environment yields nearly single-crystal C-phase films, while a low-oxygen (10^{-6} Torr) environment growth results in the formation of monoclinic polycrystalline B-phase films. Optical transmission measurements showed that the bandgap of Tb_2O_3 is direct in nature with a value of 2.8 eV and 3.4 eV for the cubic and monoclinic phases, respectively. By measuring the capacitance of test devices, quite high dielectric constants of 13.5 and 24.9 were obtained for the B- and C-phase Tb_2O_3 films, respectively. © *2014 AIP Publishing LLC*.
[http://dx.doi.org/10.1063/1.4903072]

One of the most important components in complementary metal oxide semiconductor (CMOS) devices is the gate dielectric. Silicon dioxide served as the most preferred gate oxide material for decades. However, as device features continued to decrease in size and the semiconductor industry began preparation for entering in the post-Moore era, high-k dielectrics started replacing SiO_2 gate dielectrics in CMOS devices.[1,2] A variety of different dielectrics have been examined as a replacement to SiO_2. At the present, HfO_2 is considered as the best available replacement of SiO_2. However, HfO_2 has low recrystallization temperatures, which limit the thermal budget and post-annealing processes of CMOS fabrication. Hence, HfO_2 is only considered a short term solution.[1]

Rare earth oxides are considered potential candidates for the next generation CMOS devices due to their large dielectric constants, thermal stability, and large band-offsets with silicon.[3–5] The specific rare earth oxides which have attracted the most attention so far are La_2O_3,[6] Sm_2O_3,[7] and CeO_2.[8] Tb_2O_3 is a relatively unexplored member of this family which has been predicted to exhibit a high dielectric constant.[9] In this paper, we are reporting our work on the growth and structural, optical, and dielectric characterizations of high quality Tb_2O_3 thin films.

The Tb_2O_3 thin films were produced by a pulsed laser deposition (PLD) technique. A highly dense ceramic target was made by pressing mixed valence Tb_4O_7 powder (available from Alfa Aesar) and sintering at 1400 °C for 12 h. Thin films were then deposited by ablating the densified pellet with a pulsed KrF excimer laser (wavelength: 248 nm, pulse-width: 25 ns). Films were deposited at different substrate temperatures between 500 °C and 600 °C, under (a) low O_2 pressure (10^{-6} Torr) and (b) high O_2 pressure (10^{-1} Torr). In order to test growth on a variety of substrates, films were deposited on MgO (100), $LaAlO_3$ (100), $SrTiO_3$ (100), and Si(100) single crystal substrates.

The film structures were characterized using X-ray diffraction (XRD) and cross sectional transmission electron microscopy (TEM). The optical transmission was measured using a Shimadzu model 1240 UV-Vis spectrophotometer, from which the bandgaps of the Tb_2O_3 films were calculated. Dielectric property measurements were performed on the Tb_2O_3 sandwich capacitors, where first a bottom contact layer of conductive $SrRuO_3$ was deposited onto a $SrTiO_3$ single crystal substrate by PLD. The Tb_2O_3 dielectric layer (thickness ~260 mm) was then deposited using same protocol as described earlier. Silver dots (2 mm in diameter) deposited using a shadow mask were used as the top electrodes. Frequency-dependent impedance measurements were made using a Gamry Instruments Reference 600 potentiostat up to 6 MHz, from which the capacitance values were determined and the dielectric constants of the two phases were calculated. These measurements were also confirmed using an HP 4284A precision LCR meter.

The XRD of the terbium oxide thin films grown under high (10^{-1} Torr) O_2 pressure oxygen atmosphere at 500 °C on the aforementioned substrates are shown in Fig. 1(a). From the diffraction patterns, all of these films were identified as cubic phase (C-type) Tb_2O_3. For the films grown on MgO and Si, only the (111) family of Tb_2O_3 peaks are visible, along with the (001) family of substrate peaks. In contrast, the films deposited on the $LaAlO_3$ and $SrTiO_3$ substrates showed only the (001) family of peaks from both substrate and Tb_2O_3, indicating that the film and substrate have the same c-axis orientation. In both cases, the film crystallinity was very high, with film peak intensity approximately six orders of magnitude greater than the baseline. Fig. 1(b) shows XRD scans of the Tb_2O_3 films grown under low (10^{-6} Torr) O_2 pressure with 600 °C substrate temperature on MgO, Si, $SrTiO_3$, and $LaAlO_3$. XRD patterns taken from all of these films show peaks indicating polycrystalline monoclinic phase (B-type) of Tb_2O_3 with several orientations along the substrate c-axis. From this, we conclude that oxygen pressure plays an important role determining the Tb_2O_3 film phase formed during growth.

To determine the optical properties and the bandgap of the phases, UV-Vis spectroscopy was performed on the C- and

a)Email: tiwari@eng.utah.edu

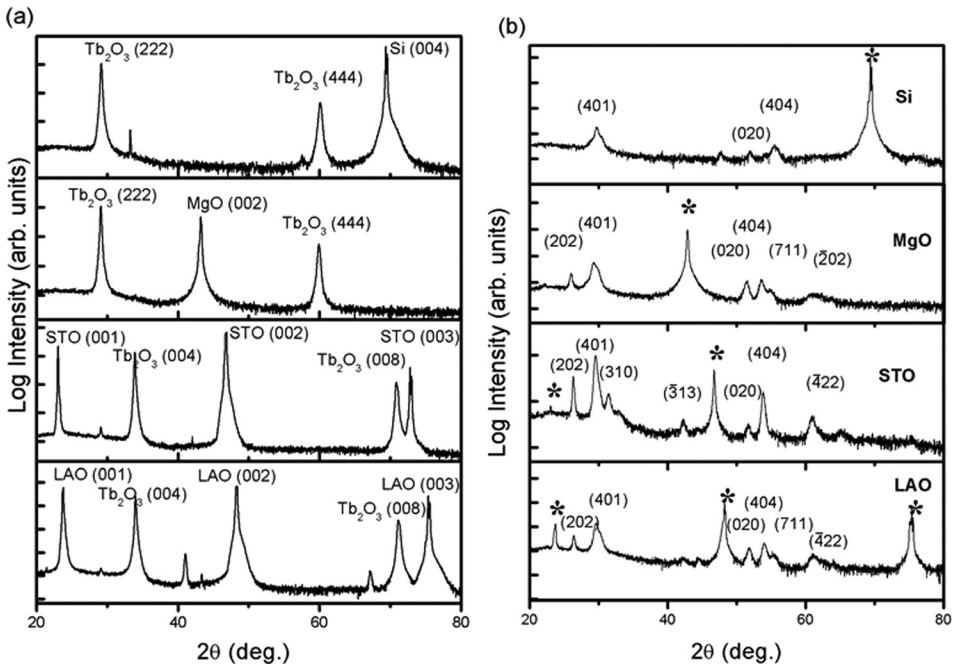

FIG. 1. XRD scan for (a) films grown on Si, MgO, $SrTiO_3$, and $LaAlO_3$ substrates under 0.1 Torr oxygen pressure, and (b) films grown on the same substrates under 1×10^{-6}Torr oxygen pressure.

B-phase Tb_2O_3 deposited on MgO. The MgO substrate was used to study optical properties because it has a very wide bandgap. The polycrystalline monoclinic phase film shows high optical transmission for wavelengths above 390 nm (Fig. 2). The bandgap was calculated by fitting absorption to the relation[10,11]

$$\alpha = C(h\nu - Eg)^n,$$

where α is absorption, n = 1/2 for direct bandgaps, Eg is the energy bandgap, ν is the frequency, h is Planck's constant, and C is a constant. From the absorption spectra, the bandgap of B-phase monoclinic Tb_2O_3 was estimated to be 3.9 eV. This value is quite consistent with other literature on polycrystalline Tb_2O_3.[12] This energy gap is understood to originate the transition from the localized filled f-level in Tb sitting above the valence band (O 2p) to the unoccupied Tb 5d conduction band.[13,14] The cubic phase Tb_2O_3 thin film shows a reduced bandgap, calculated by the above method to be 2.7 eV.

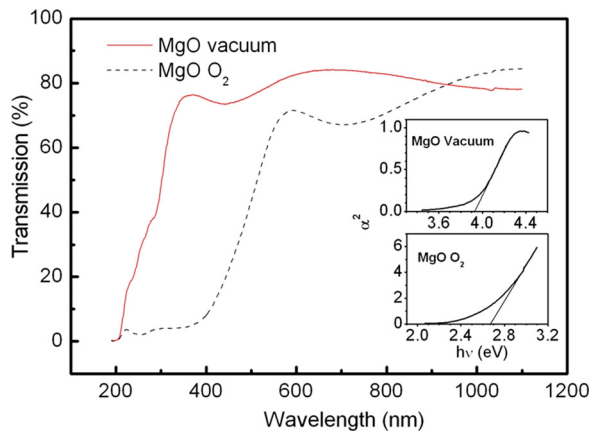

FIG. 2. Optical transmission spectrum of Tb_2O_3 thin films grown on MgO substrate under O_2 and vacuum. Insets show bandgap calculation by plotting absorption α^2 vs hν.

Cross sectional TEM, including low magnification bright field TEM, high resolution TEM (HRTEM), and selected area diffraction (SAD), was performed on the Tb_2O_3 thin film samples grown under high oxygen pressure in order to study the crystal growth and quality in detail. The bright field images of both films show a clean interface with no obvious signs of intermixing. Thickness measured by bright field imaging was ~260 nm for both films grown on STO and MgO.

Fig. 3(a) shows the SAD pattern of the C-phase Tb_2O_3 film grown on $SrTiO_3$ substrate. From the diffraction pattern, the out of plane orientation relationship $(002)_{substrate}||(004)_{terbium\ oxide}$ is confirmed. The zone axis of the film is identified as [001], and substrate zone axis as [110], giving the in plane orientation $(110)_{substrate}||(100)_{terbium\ oxide}$. This indicates that the film grows on $SrTiO_3$ via domain-matching epitaxy[15] with a 45° in-plane rotation with respect to the substrate. In this direction, two of the substrate ($SrTiO_3$) lattice spaces approximately match to one Tb_2O_3 lattice space. By this growth mechanism, the calculated misfit is less than 3% for $SrTiO_3$. Films grown on $LaAlO_3$ have the same orientation and therefore should share the same growth mechanism, having a calculated lattice mismatch of about −0.01%. Fig. 3(b)

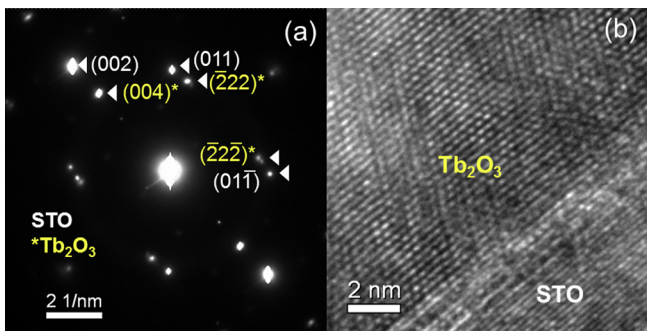

FIG. 3. (a) SAD pattern of Tb_2O_3 film on $SrTiO_3$ substrate showing the film's [100] zone axis and the substrate's [110] zone axis. (b) HRTEM of interface between the Tb_2O_3 film and the $SrTiO_3$ substrate.

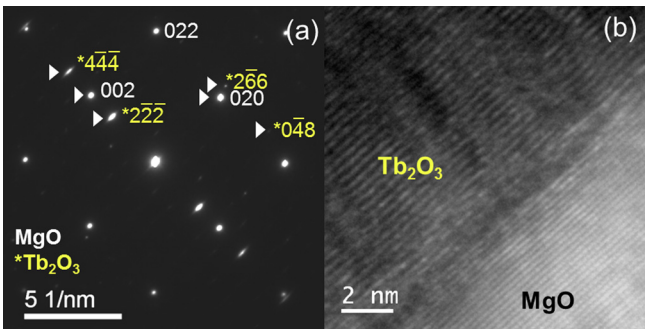

FIG. 4. (a) SAD pattern of Tb_2O_3 film on MgO substrate showing the film's [321] zone axis and the substrate's [100] zone axis. (b) HRTEM of interface between the Tb_2O_3 film and the MgO substrate.

shows high resolution TEM of the $Tb_2O_3/SrTiO_3$ interface. The film appears to form a coherent interface with the substrate, with no obvious grain boundaries or impurities, indicating good crystallinity.

Fig. 4(a) shows SAD for Tb_2O_3 grown on an MgO substrate. Out of plane orientation of this film is characterized by $(002)_{substrate}||(222)_{Tb_2O_3}$. The indexed zone axes are [100] for the substrate and [321] for the film, giving in-plane orientation to be $(100)_{substrate}||(321)_{Tb_2O_3}$. SAD patterns from both films on the MgO and the $SrTiO_3$ confirm very high quality oriented crystal growth, with little to no misalignment in orientation. The HRTEM shown in Fig. 4(b) for the Tb_2O_3/MgO interface again shows an abrupt interface and a constant orientation between the film and substrate. Some contrast changes in this image may be due to line defects, but are likely due to damage from local heating introduced during sample preparation by milling with focused ion beam, which was seen throughout this film and substrate. Since the X-ray diffraction pattern of films grown on MgO was identical to those grown on Si substrates, the orientation relationships of both films are assumed to be the same.

Figure 5 shows the dielectric constant measured as a function of frequency up to 1 MHz, with dissipation loss factor, D, for both cubic and monoclinic films. There is some variation with frequency, as is apparent with the dip in k and higher loss, D at around 600 kHz due to some parasitic factors. At this point, there is a higher loss in the monoclinic thin films, attributed to the polycrystalline nature of the film in which grain boundaries contribute to capacitance leakage.[16] At all frequencies, the highly oriented cubic film shows a much greater dielectric constant than the monoclinic films, and is almost double at low frequencies. Specifically, the measured dielectric constant of monoclinic Tb_2O_3 films at 100 kHz is $k = 13.5$ while the highly crystalline cubic thin films show an enhanced dielectric constant of $k = 24.9$ at the same frequency.

To summarize, we have grown high quality Tb_2O_3 thin films with different crystallographic orientations on a variety of substrates. Under high oxygen pressure, we have shown the growth of nearly single crystal C-phase thin films, which

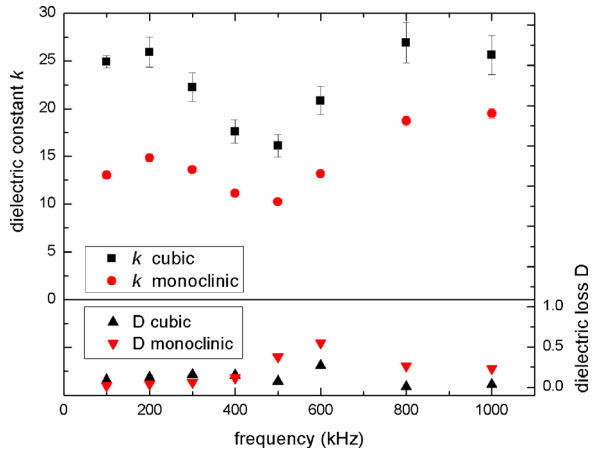

FIG. 5. (Top) Dielectric constant measurements of cubic and monoclinic Tb_2O_3 thin films as varied with frequency. Error bars show standard error. (Bottom) Dielectric loss $D = \tan\delta$ for both the cubic and monoclinic samples.

can be grown either in (001) or (111) orientation depending on the choice of the substrate. Using low oxygen pressure, a different crystal structure B-phase monoclinic Tb_2O_3 was achieved. These results were confirmed using X-ray diffraction and high resolution TEM. We have also illustrated that the dielectric constant varies significantly between the C- and B-phase of Tb_2O_3, decreasing by a factor of 1.8, i.e., from 24.9 to 13.5 for C- and B-phase, respectively.

Financial support from the National Science Foundation through Grant Nos. 1121252 (MRSEC) and DMR-0746486 (CAREER) is thankfully acknowledged.

[1]ITRS Homepage, International Technology Roadmap for Semiconductors, 2013. See www.itrs.net.
[2]J. H. Choi, Y. Mao, and J. P. Chang, Mater. Sci. Eng., R **72**, 97 (2011).
[3]K. J. Hubbard and D. G. Schlom, J. Mater. Res. **11**, 2757 (1996).
[4]*Rare Earth Oxide Thin Films: Growth, Characterization, and Applications*, edited by M. Fanciulli and G. Scarel (Springer, 2010).
[5]M. Leskelä, K. Kukli, and M. Ritala, J. Alloys Compd. **418**, 27 (2006).
[6]J. Päiväsaari, M. Putkonen, and L. Niinistö, Thin Solid Films **472**, 275 (2005).
[7]H. Yang, H. Wang, H. M. Luo, D. M. Feldmann, P. C. Dowden, R. F. DePaula, and Q. X. Jia, Appl. Phys. Lett. **92**, 062905 (2008).
[8]Y. Nishikawa, T. Yamaguchi, M. Yoshiki, H. Satake, and N. Fukushima, Appl. Phys. Lett. **81**, 4386 (2002).
[9]D. Xue, K. Betzler, and H. Hesse, J. Phys.: Condens. Matter **12**, 3113 (2000).
[10]*Semiconductors and Semimetals*, edited by R. K. Willardson and A. C. Beer (Academic, New York, 1967), Vol. 3, Chap. 6.
[11]M. Snure and A. Tiwari, Appl. Phys. Lett. **91**, 092123 (2007).
[12]A. V. Prokofiev, A. I. Shelykh, and B. T. Melekh, J. Alloys Compd. **242**, 41 (1996).
[13]L. Petit, A. Svane, Z. Szotek, and W. M. Temmerman, Phys. Rev. B **72**, 205118 (2005).
[14]H. B. Lal and K. Gaur, J. Mater. Sci. **23**, 919 (1988).
[15]J. Narayan and B. C. Larson, J. Appl. Phys. **93**, 278 (2003).
[16]G. D. Wilk, R. M. Wallace, and J. M. Anthony, J. Appl. Phys. **89**, 5243 (2001).